

LA-UR-80-2830

CONF - SEICGS - 9

TITLE: A ROTATING PENNING SURFACE-PLASMA SOURCE FOR DC H<sup>-</sup> BEAMS

AUTHOR(S): H. Vernon Smith, Jr., Paul Allison, and Joseph D. Sherman

SUBMITTED TO: Second International Symposium on the Production and Neutralization of Negative Hydrogen Ions and Beams, Brookhaven National Laboratory, Upton, L.I., October 6-10, 1980.

**MASTER**

University of California

DISCLAIMER

This document is prepared for the U.S. Government under contract number W-7408-ENG-36. The U.S. Government is authorized to reproduce and distribute reprints for government purposes not withstanding any copyright notation that may appear hereon. This document is the property of the U.S. Government and is loaned to your organization; it and its contents are not to be distributed outside your organization.

By acceptance of this article, the publisher recognizes that the U.S. Government retains a nonexclusive, royalty-free license to publish or reproduce the published form of this contribution, or to allow others to do so, for U.S. Government purposes.

The Los Alamos Scientific Laboratory requests that the publisher identify this article as work performed under the auspices of the U.S. Department of Energy.



**LOS ALAMOS SCIENTIFIC LABORATORY**

Post Office Box 1663 Los Alamos, New Mexico 87545

An Affirmative Action/Equal Opportunity Employer

## A ROTATING PENNING SURFACE-PLASMA SOURCE FOR DC H<sup>-</sup> BEAMS\*

H. Vernon Smith, Jr., Paul Allison, and Joseph D. Sherman  
AT-2 (MS-818), Los Alamos Scientific Laboratory  
Los Alamos, NM 87545

### Abstract

We investigate the possibility of using a Penning surface-plasma source (SPS) with rotating electrodes to produce dc H<sup>-</sup> beams. In this rotating ion source (RIS), the average power density on the electrodes is reduced by magnetically confining the discharge to a small region near the emission slit while maintaining the geometry and instantaneous power density of the fixed-electrode Penning SPS. H<sup>-</sup> beam currents (2.5 mA at 100% duty factor, 104 mA at 1.5% duty factor) and two-dimensional normalized emittances (0.036  $\pi$  cm·mrad  $\times$  0.009  $\pi$  cm·mrad for 40% of a 1.5-mA, dc H<sup>-</sup> beam) similar to those of the fixed-electrode Penning SPS are produced by the uncooled RIS reported in this paper. The scaling to a 100% duty factor, fully cooled RIS is briefly discussed.

### I. Introduction

New linac structures, such as the radio-frequency quadrupole (RFQ)<sup>1</sup>, may allow a substantial increase in the average beam current injected into particle accelerators. We are developing a rotating Penning surface-plasma source (SPS)<sup>2</sup> as a high current (~100 mA), dc H<sup>-</sup> source for this application. We chose to build a Penning SPS because of (1) its low emittance and (2) its adaptability to a design employing rotating electrodes.

Using the source magnetic field we confine the rotating ion source (RIS) discharge to a small region near the emission slit, thereby reducing the average electrode heat load by the ratio of the discharge length to the electrode circumference, about a factor of 40. We built and tested the uncooled RIS described in this paper. We find that it produces H<sup>-</sup> beams similar in quality to those generated by the fixed-electrode Penning SPS<sup>3,4</sup>.

### II. Source Design

In developing an ion source to produce ~100 mA of H<sup>-</sup> at 100% duty factor and an emission density  $J^- = 2$  A/cm<sup>2</sup>, we find it necessary to add the complication of rotating electrodes because of power loading considerations. In our fixed-electrode Penning SPS<sup>3</sup>, 110-mA H<sup>-</sup> current pulses are produced by discharge current and voltage pulses of 60 A and 80 V, respectively, corresponding to  $J^- = 2.2$  A/cm<sup>2</sup> through the 0.5-mm by 10-mm emission slit. Because the ratio of cathode power to anode power is about 2 at a discharge voltage of 100 V (Ref. 5), the 4.8-kW pulsed discharge

power is equally shared by the anode and each of the two cathodes. The exposed cathode surface (0.48 mm<sup>2</sup>) has a 6.7-kW/cm<sup>2</sup> heat load, about an order of magnitude too high for operation at 100% duty factor. The exposed anode surface (0.7 cm<sup>2</sup>) has a 2-kW/cm<sup>2</sup> power load, still about a factor of 4 too high. It is desirable to reduce these heat loads to 0.5 kW/cm<sup>2</sup> or less. Reducing the electrode power loading by enlarging the source dimensions might lead to a reduced emission density and thus a lower H<sup>-</sup> beam brightness.<sup>6</sup>

The RIS design (Fig. 1) maintains the geometry and instantaneous power density of the fixed-electrode source.<sup>3,6</sup> Because the SPS discharge will not operate below a minimum magnetic field  $B_m$ , the spatial extent of the RIS discharge is controlled by the magnet pole piece shape (1 cm by 1 cm) and the current in the electromagnet coils. The average RIS electrode power density is reduced by the ratio of the length of the discharge region (~1.2 cm) to the circumference of the electrodes (44 cm), about a factor of 37. The RIS design calls for a 100-V, 100-A discharge, resulting in anticipated power densities of 380 W/cm<sup>2</sup> for the cathodes and 150 W/cm<sup>2</sup> for the anode, well within the limits of cooling with present technology.

Initially, both RIS cathodes and the anode were rotated. For reasons discussed below, we presently rotate only the cathodes; the rotating anode (Fig. 2b) was replaced with a fixed structure (Fig. 2c). Ferrofluidic feedthrus<sup>7</sup>, using magnetic-fluid seals, provide the rotating shaft seals. Discharge power is transferred to the shafts by carbon brushes. The shaft drive motor is at ground potential and has variable speed. The anode and cathodes are constructed from molybdenum, the source housing from stainless steel.

Because the fixed-electrode source operates for at least 1 ms with 100-mA H<sup>-</sup> yields, the 1.2-cm-long arc slot results in an upper limit of 1200 cm/s for the electrode speed in the RIS. The 14-cm RIS electrode diameter sets the required rotational speed at < 1600 rpm. Measurements show negligible braking of the drive motor by eddy currents induced in the rotating electrodes (< 20 W at 1700 rpm). The magnetic field in the discharge region changes by < 5% when the source rotational speed is varied from 0 to 1700 rpm.

Four electrical cartridge heaters are used to heat the source body to 250°C, thereby limiting cesium condensation on the inner surfaces of the source housing. Cesium metal vapor is

\*Work performed under the auspices of the U.S. Department of Energy.

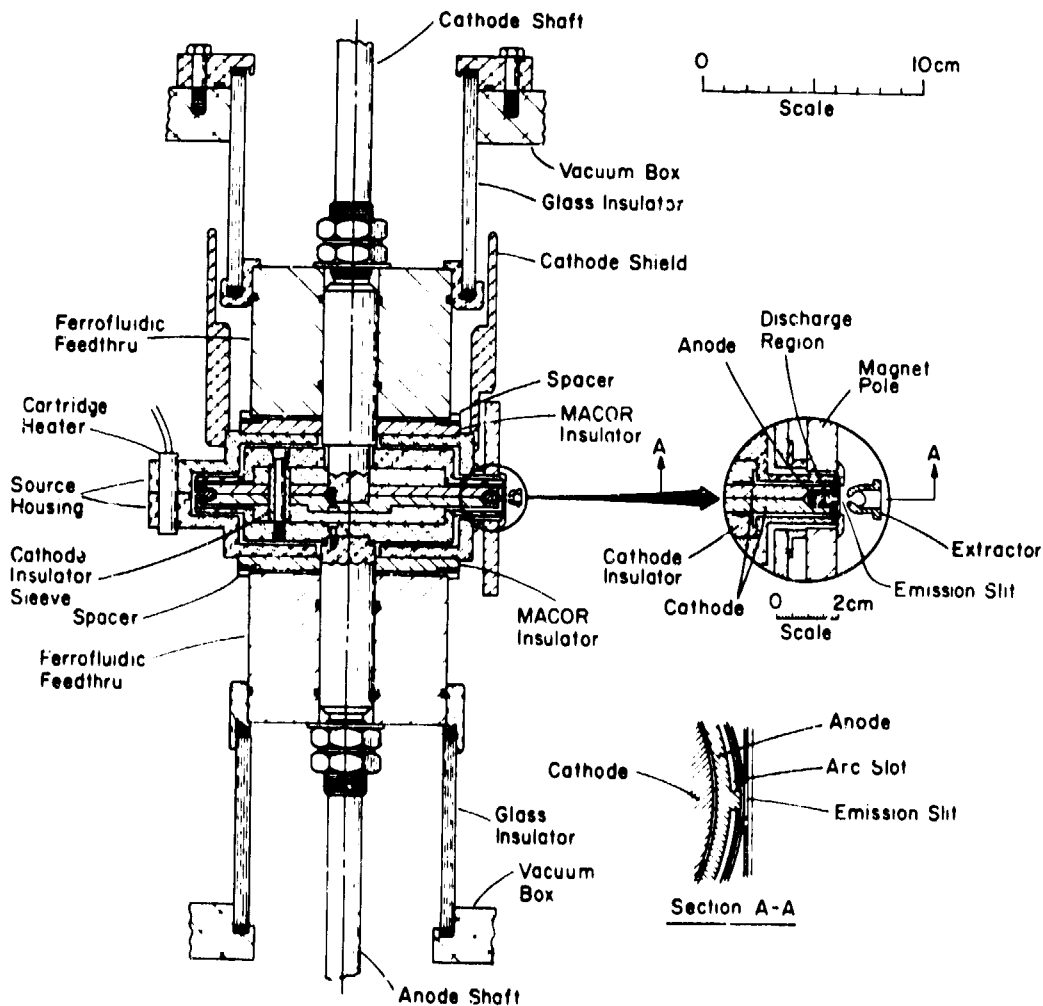


Fig. 1. The rotating ion source.

Table I. Design and Achieved H<sup>-</sup> Performance Levels in the RIS.

	Design	DC	Pulsed
Discharge current, A	100	1.0	98
Discharge voltage, V	100	160	100
H <sub>2</sub> flow, sccm	-	36	115
Magnetic field, T	-	0.14	0.15
Rotational speed, rpm	-	120	15
Duty factor, %	1	100	1.5
Beam energy, keV	20	10.1	21
H <sup>-</sup> current, mA	~100	1.5	104*
J <sup>-</sup> , A/cm <sup>2</sup>	~2	0.03	2.1*
$\epsilon_x(63\%) \times \epsilon_y(63\%)$ , n <sup>2</sup> cm <sup>2</sup> mrad <sup>2</sup>	-	0.036x0.009	-
B(40%), A/cm <sup>2</sup> mrad <sup>2</sup>	-	0.91	-
H <sup>-</sup> conversion efficiency, A of H <sup>-</sup> /A of arc	> 0.001	0.0015	0.0011*
Thermal efficiency, kW of arc/A of H <sup>-</sup>	< 100	107	94*

\*Unanalyzed.

injected in the source housing 215° around the electrode wheel from the discharge region. The cesium metal feed (similar to that in Fig. 2 of Ref. 8) incorporates an all-metal, bellows-sealed needle valve for adjustment of the cesium flow rate. Presently we do not cool either the emission slit (0.5 by 10 mm<sup>2</sup>) or the extraction electrode. The ion source test stand and electrical supplies used to test<sup>3,6</sup> the fixed-electrode source are used for the RIS. The design H<sup>-</sup> performance levels for the RIS are given in column 1 of Table I.

### III. Results and Discussion

Because the RIS design relies on the discharge magnetic field to limit the length of the discharge region along the electrode periphery, it is important to confirm this effect. To do this, we constructed a special rotating anode, containing only two 2-mm-wide by 5-mm-long arc slots located 180° apart (Fig. 3a). We used pole pieces with 1-cm square faces. The source electrode wheel was rotated at moderate speed

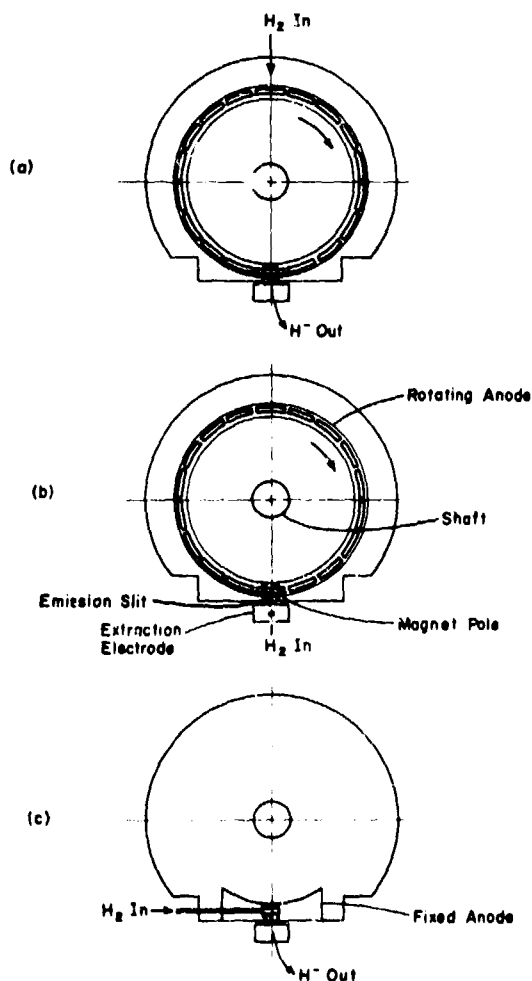


Fig. 2. (a) Schematic of the original H<sub>2</sub> gas feed, located 180° around the electrode wheel from the discharge region. (b) Capillary H<sub>2</sub> gas feed through the emission slit. (c) Fixed anode structure, with H<sub>2</sub> gas fed directly into the arc slot.

to pass the arc slots through the discharge region at 16 Hz. A timing pulse indicated a fixed location on the electrode periphery so that we could measure the rate of rotation. We then measured the discharge and H<sup>-</sup> currents as a function of wheel location (Fig. 3b). These measurements were repeated for many different settings of the magnetic field. As shown in Fig. 3c, the width of the discharge region decreases monotonically with magnetic field. A 0.1-T field produced a 1-cm discharge width. Thus, the spatial extent of the RIS discharge can be controlled with the magnetic field for discharge currents near 1 A.

We varied the location of the H<sub>2</sub> gas feed as shown in Fig. 2. Feeding H<sub>2</sub> gas into the

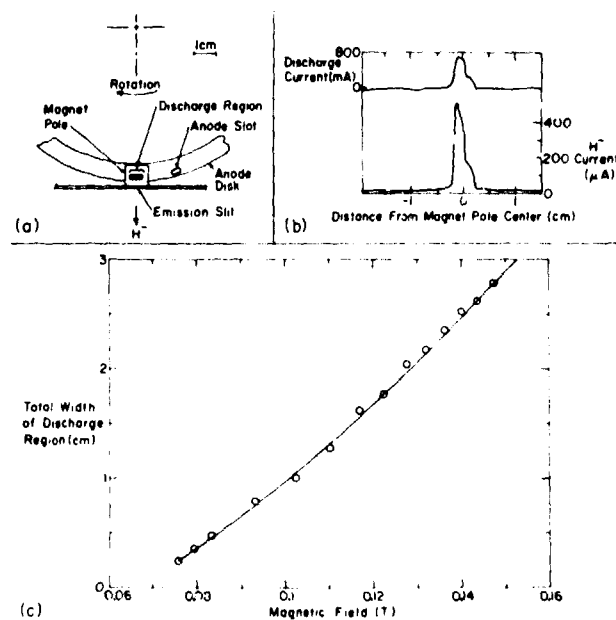


Fig. 3. (a) The magnet poles and the anode used to measure the width of the discharge region as a function of magnetic field strength. (b) The discharge current (top) and H<sup>-</sup> current (bottom) as a function of the location of the 5-mm-long arc slot for a 0.084-T magnetic field. (c) The total width of the discharge region vs the discharge magnetic field strength. The curve serves only to guide the eye.

source housing 180° from the discharge region (Fig. 2a) is a satisfactory arrangement for dc operation at 1 A of discharge current. However, with this arrangement the RIS only operates stably for pulsed discharge currents < 20 A. At higher discharge currents the voltage and current oscillate at ~ 10 kHz with 100% modulation. We calculate that at the higher currents the discharge can pump the H<sub>2</sub> gas away in < 10 μs. Perhaps this causes the instabilities. To investigate this possibility, a 0.4-mm-i.d. capillary tube was directed into the discharge region through the emission slit and used as the H<sub>2</sub> gas feed (Fig. 2b). Steady operation at discharge currents up to 80 A resulted. We then replaced the rotating anode with a fixed anode structure (Fig. 2c) and fed the H<sub>2</sub> gas directly into the arc slot as in the fixed-electrode source. This change allowed steady pulsed operation at discharge currents up to 120 A. All measurements reported below were obtained using the fixed-anode structure. The pulsed H<sup>-</sup> current increased when the number of H<sub>2</sub> gas inlets in the fixed anode was increased from one to five, the five inlets being equally spaced along the 1.2-cm arc slot.

Because of the need to support the rotating anode, the drift distance  $t$  (see inset in Fig. 4) from the arc slot to the emission slit was 2 mm in the RIS compared to 1 mm in the fixed-electrode source. We studied the effect of varying  $t$  on the  $H^-$  output of the fixed-electrode source and found that it is an important parameter (open circles and curve in Fig. 4). Using two different fixed anodes, we measured the pulsed  $H^-$  output from the RIS with  $t = 2$  mm and  $t = 1/2$  mm and found that  $t = 1/2$  mm gives the best  $H^-$  output (squares, Fig. 4). The RIS current and emittance measurements reported below were all obtained for  $t = 1/2$  mm.

The cesium flow through the RIS emission slit is monitored using a cesium surface-ionization gauge (SIG) identical to that described in Ref. 9. Typically, the cesium flow from the RIS is identical to that measured for the fixed-electrode source (see Figs. 2-4 of Ref. 9), 1 mg/h for dc operation at 1 A discharge current.

The  $H^-$  current and two-dimensional, normalized emittance ( $\epsilon = B\gamma A/\pi$ , where  $A$

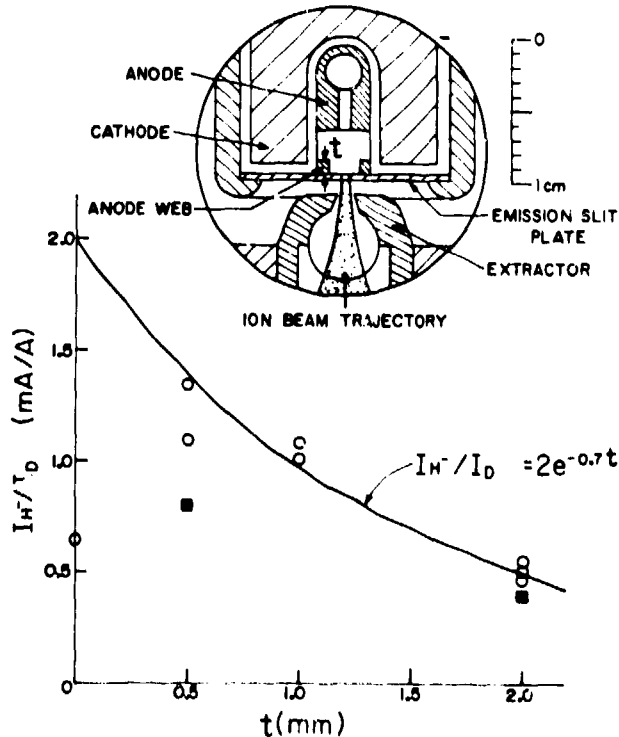


Fig. 4. The ratio of  $H^-$  current to pulsed discharge current ( $I_D \sim 100$  A) vs the distance from the arc slot to the emission slit  $t$  (inset) for the fixed electrode source (circles) and the RIS (squares). The curve is calculated assuming an exponential attenuation of  $H^-$  ions in the drift  $t$ . The  $1/e$  attenuation distance is 1.4 mm.

is the phase-space area of the beam and  $B$  and  $\gamma$  are the relativistic parameters) for dc RIS operation are shown in Table I. The largest dc RIS  $H^-$  beam we have observed is 2.5 mA, for which we have no emittance measurements. Figure 5 shows  $\epsilon$  as a function of the beam-current fraction  $I/I_0$  for the 1.5-mA dc beam. The  $x, \theta$  direction is parallel to the 0.5-mm by 10-mm emission slit and in the bending plane of the  $n = 0.9$  dipole magnet; the  $y, \phi$  direction is perpendicular to the slit.

The data displayed in Fig. 5 were obtained in the following manner. The emittance scanner<sup>2</sup> was set at a fixed position  $x$ , then an oscillogram of the emittance scanner Faraday-cup current  $S_x$  vs the emittance scanner plate sweep voltage (proportional to  $\theta$ ) was recorded. The emittance scanner was stepped across the beam to record the three-dimensional plot of  $S_x$  vs  $x$  and  $\theta$ . Because  $S_x = \partial^2 I / \partial x \partial \theta$ , the integral

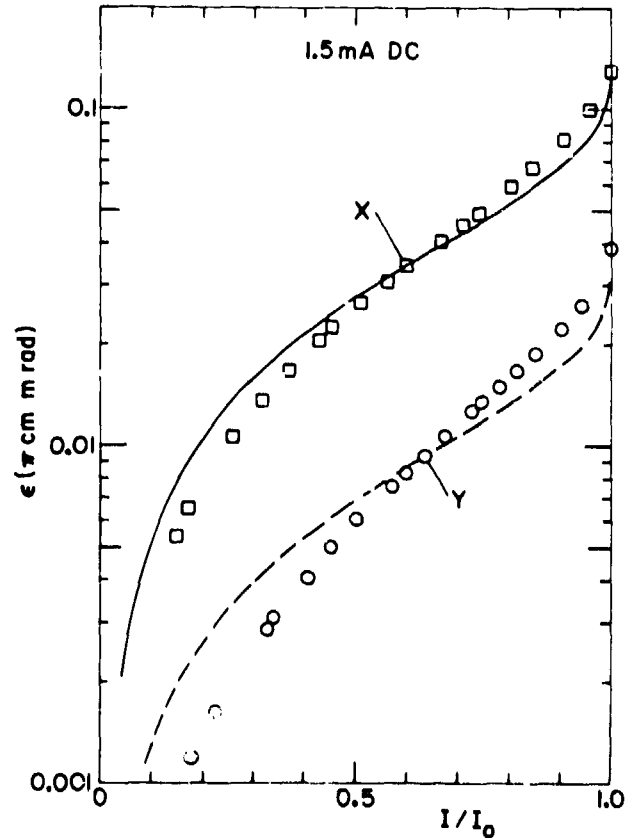


Fig. 5. Two-dimensional, normalized emittance  $\epsilon$  vs the fraction of the total beam included in the emittance measurement  $I/I_0$  for a 1.5-mA dc  $H^-$  beam from the RIS. The curves are calculated from Eq. (2) assuming  $kT_x = 3.7$  eV (solid curve) and  $kT_y = 96$  eV (dashed curve).

$I_1 = \int \partial^2 I / \partial x \partial \theta d\theta$  is the beam profile. The integral  $I_2 = \int \partial^2 I / \partial x \partial \theta d\theta dx$  is proportional to the total beam current  $I_0$ . A computer program calculates the normalized emittance and beam current included at various threshold (brightness) levels. These results then permit plotting normalized emittance  $\epsilon(F)$  vs the beam current fraction ( $F=I/I_0$ ). A second, identical emittance scanner is used to make the  $y, \phi$  emittance measurements. The normalized brightness  $B(F^2)$  is calculated from

$$B(F^2) = 2 I_0 / [\pi^2 \epsilon_x(F) \epsilon_y(F)] \quad (1)$$

The values of  $\epsilon$  given in Table I correspond to the emittance value that includes 63% of the beam in each plane, or 40% of the total beam. The discharge voltage noise to discharge voltage ratio was 0.14 for these measurements. The dc  $H^-$  current, emittance, and brightness values for the RIS and the fixed-electrode source ( $I_0 = 2$  mA,  $\epsilon_x \times \epsilon_y = 0.044 \times 0.016 \pi^2 \text{cm}^2 \text{mrad}^2$ ,  $B=0.58 \text{ A/cm}^2 \text{mrad}^2$ ,  $F=63\%$ , Table IV of Ref. 10) are very similar at the  $\sim 2$ -mA level.

The largest pulsed RIS  $H^-$  beam we have measured is 104 mA (Table I). The maximum field strength provided by the dipole magnet is insufficient to bend a 21-keV  $H^-$  beam through  $90^\circ$  and into a Faraday cup for measurement. The 104 mA was recorded in a Faraday cup located 2 cm behind the extraction electrode, without magnetic analysis of the beam.

We have not yet obtained emittance measurements for the RIS pulsed beam. However, the dc current, emittance, and brightness values for the RIS are so similar to those for the fixed-electrode source that we expect a 100-mA pulsed  $H^-$  beam from the RIS to have nearly the same emittance and brightness as the fixed-electrode source ( $I_0 = 79$  mA,  $\epsilon_x \times \epsilon_y = 0.041 \times 0.027 \pi^2 \text{cm}^2 \text{mrad}^2$ ,  $B = 15 \text{ A/cm}^2 \text{mrad}^2$ ,  $F = 63\%$ , Fig. 6 of Ref. 11).

From a model<sup>11</sup> that assumes the  $H^-$  ions are emitted uniformly from the rectangular emission slit with a Maxwellian velocity distribution of temperature  $T$ , the beam fraction vs normalized emittance is given by

$$F = \text{erf} [\pi \epsilon / \{4R (2kT/mc^2)^{1/2}\}] \quad (2)$$

where  $R$  is half the slit dimension and  $m$  is the ion mass. The curves in Fig. 5 were calculated using Eq. (2), normalized to the values of  $\epsilon$  at  $F = 3\%$ . Using the values of  $\epsilon_x$  (63%),  $\epsilon_y$  (63%), and Eq. (2), we obtain estimates of the ion energy of  $kT_x = 3.7$  eV and  $kT_y = 96$  eV. We know<sup>12</sup> that the dipole magnet pole pieces couple the  $x$ - and  $y$ -plane emittances, so the larger emittance of the  $x$ -plane masks that of the  $y$ -plane. The larger effective ion energy reflects the small initial plasma radius for the  $y$ -plane.

The principal difference noted between the operation of the RIS and the fixed-electrode source is that for maximum dc  $H^-$  current, the discharge voltage for the RIS is 170 V, compared to 50 V for the fixed-electrode source. The difference in discharge voltage for pulsed operation is not so great; 100 V for the RIS compared to 80 V. We do not understand the difference in operating voltage. Understanding and controlling the voltage has clear implications for a fully cooled RIS, because a lowering of the discharge voltage reduces the electrode heat load by the same factor.

#### IV. Summary and Conclusions

We have shown that magnetic-field confinement of the Penning SPS discharge can be used to reduce the average heat load on the cathodes in a rotating source design. Using a fixed anode and rotating cathodes in our uncooled RIS, we have achieved performance levels at 1-mA  $H^-$ , 100% duty factor and 100-mA  $H^-$ , 1% duty factor which are comparable to those of the fixed-electrode Penning SPS described in Refs. 3 and 6.

A fully cooled RIS must have adequate cooling for the anode and both cathodes, the emission slit, and the extraction electrode. Taking our pulsed RIS measurements (Table I), correcting for 30% attenuation of the  $H^-$  beam when it is magnetically analyzed, and scaling up to 100 mA of analyzed  $H^-$  beam implies that each rotating cathode will have a power load of 0.5 kW/cm<sup>2</sup>, the anode 0.16 kW/cm<sup>2</sup> if rotated and 6 kW/cm<sup>2</sup> if fixed. The power loading on the extraction electrode may be a serious problem because a 20-keV, 100-mA  $H^-$  beam having a 2-A/cm<sup>2</sup> current density has an average power density of 40 kW/cm<sup>2</sup>. This scaling to a fully cooled, 100% duty factor RIS is acceptable, provided the anode and extraction electrode heat loads can be reduced.

#### References

1. R. H. Stokes, K. R. Crandall, R. W. Hamr, F. J. Humphry, R. A. Jamson, E. A. Knapp, J. M. Potter, G. W. Rodenz, J. E. Stovall, D. A. Swenson, and T. P. Wangler, paper presented at the XIth Int. Conf. on High Energy Accelerators, CERN, Geneva (July, 1980); and LA-UR-80-1855.
2. The physics of SPS sources is discussed in: Yu. I. Bel'chenko, G. I. Dimov, and V. G. Dudnikov, Proc. of the Symp. on the Production and Neutralization of Negative Hydrogen Ions and Beams, BNL-50727, pp 79-95 (September, 1977).
3. P. W. Allison, in Ref. 2, pp 119-122.

4. G. E. Derevyankin and V. G. Dudnikov, Institute of Nuclear Physics Preprint IYAF 79-17, Novosibirsk, 1979 (UCRL-TRANS-11549).
5. Yu. I. Bel'chenko and V. G. Dudnikov, Conf. on Interactions of Atomic Particles in Solid Bodies, Kharkov, 1976 (Scientific Translation Service Inc., 1976, Trans. 4 pp).
6. P. W. Allison, IEEE Trans. on Nucl. Sci. NS-24, 1594-1596 (1977).
7. Model No. SC-1000-N-W-Modified, manufactured by Ferrofluidic Corp., Burlington, MA 01803.
8. H. V. Smith, Jr., Nucl. Instr. and Methods 164, 1-10 (1979).
9. H. V. Smith, Jr., and P. W. Allison, IEEE Trans. on Nucl. Sci. NS-26, 4006-4008 (1979).
10. J. D. Sherman, P. Allison, and H. V. Smith, Jr., Proc. of this Conf.
11. P. Allison, H. V. Smith, Jr., and J. D. Sherman, Proc. of this Conf.
12. J. D. Sherman and P. W. Allison, IEEE Trans. on Nucl. Sci. NS-26, 3916-3918 (1979).